J Solid State Electrochem (2012) 16:2733–2738
DOI 10.1007/s10008-012-1690-y

ORIGINAL PAPER

Si/C nanocomposite anode materials by freeze-drying with enhanced electrochemical performance in lithium-ion batteries

Xing Xin · Xiayin Yao · Yiming Zhang · Zhaoping Liu · Xiaoxiong Xu

Received: 14 December 2011 / Revised: 8 February 2012 / Accepted: 13 February 2012 / Published online: 3 March 2012

Abstract The nanostructured Si/graphite composites embedded with the pyrolyzed polyethylene glycol was synthesized from coarse silicon and natural graphite by a facile and cost-effective approach. The Si/C nanocomposite showed the fluffy carbon-coated structure, which was confirmed by the SEM and TEM measurements. The as-obtained Si/C nanocomposite, employed as anode material in lithium-ion batteries, exhibited significantly enhanced rate capability and cycling stability. The improved electrochemical stability of the composite was evaluated by EIS and galvanostatically charge/discharge test. A reversible capacities as high as 85% and 91% of the initial charge capacities, could be maintained for the Si/C nanocomposite electrode after 40 cycles under the high current densities of 500 and 1,000 mA g^{-1}, respectively. The relatively low cost and excellent electrochemical capability of the Si/C nanocomposite would well meet the challenge in rapid charge and discharge for large-size lithium-ion rechargeable batteries.

Keywords Si/C nanocomposite anode · High-rate capability · Capacity retention · Lithium-ion batteries

Introduction

Lithium-ion batteries (LIBs) have been successfully commercialized for over 20 years, however, further improvements are still needed to meet the demands for high power applications such as electric vehicles (EVs) and plug-in hybrid electric vehicles [1]. From this perspective, the widely used graphite, which is predominantly used as the anode material in LIBs, has been operating close to their theoretical capacity limits. In order to further enhance battery performance, new anode materials have been widely sought. In the past decade, substantial efforts have been made to exploit silicon-based electrodes owing to its abundance in nature, low charge potential, and its high theoretical capacity of 4,200 mA h g^{-1} which is ten times higher than their carbon-based counterparts [2–6]. Nevertheless, the well-known disadvantages limit the practical application of silicon-based material [7–9]. The dramatic volume change of Si during lithiation and delithiation leads to mechanical failure of the anode and crumbling of the electrodes, resulting a very poor cycle life. In addition, the low electronic conductivity of pristine Si makes it difficult to achieve good electrochemistry performance at a high current density.

In recent years, many attempts have been made to improve electrochemical performance of Si-based anode. It is no doubt that minimization of the size to nanoscale of Si-based electrode was an efficient approach to improve the cycling stability and high-rate capability due to alleviation of the volume variation during cycling and shortened the pathway for Li^+ ions to rapidly transport [5, 10–13]. However, the nanosilicons, such as silicon nanowires, silicon films, and silicon nanocrystals, are difficult to be synthesized in large scale. Another generally accepted strategy to alleviate the disadvantages is to prepare Si/C nanocomposite. Graphite, mesophase microbeads, pyrolyzed polyvinyl chloride, and other carbonaceous materials have been used as carbon source for Si-based anode materials [14–16]. The carbon phase in the Si/C composites acts as both of a structural buffer and an electrochemically active material because of its softness, good electronic conductivity, and much smaller volume expansion [17–19]. Numerous

X. Xin · X. Yao · Y. Zhang · Z. Liu · X. Xu (✉)
Ningbo Institute of Material Technology and Engineering,
Chinese Academy of Sciences,
Ningbo 315201, People's Republic of China
e-mail: xuxx@nimte.ac.cn

methods have been employed in preparing Si/C composite anodes, including mechanical milling, chemical/thermal vapor deposition, and the sol–gel method [18, 20, 21]. All of the strategies focused on creating the suitable structure to limit the volume change of Si-based composites during the charge and discharge. J. Yang [17] utilized the polyvinyl as a carbon precursor to coat the Si anode and obtained a Si/C anode material with high reversible capacity and improved cycle stability. Wang et al. [22] dispersed the Si nanocrystals into carbon aerogel to alleviate the volume variation of the pure Si electrode during cycling. The novel nano-Si/C composite demonstrate good cyclability at a rate of 0.1 C.

Hence, it is believed that embedding the nano-Si into the carbon matrix homogenously could improve the performance of Si-based anode material. However, the practical applications of the mixtures of silicon nanoparticles and carbon matrix are not so wide because nano-Si is difficult to be coated by carbon without any pretreatment due to its large surface stress [23]. Until now, there are few studies to report synthesizing the Si/C nanocomposite as the anode material through a simple and large-scale route. Comparing with the above methods of preparing the nanosized Si/C composite, the freeze-drying is a classical technique which has been successfully used in preparation of nanostructured materials [24]. This process can be divided into two stages: rapidly freezing a solution and vacuum drying to remove water in the solution at low temperatures. The particle aggregations can be obviously eliminated during the freeze-drying process, after various kinds of components in the composites are homogeneously mixed. Adopting the freeze-drying method to prepare the Si/C nanocomposite is much possible to be a good attempt.

In this paper, we report an industrially oriented approach to realize the fluffy carbon-coated structure for the Si/C composite electrode material through high-energy shaker milling and freeze-drying. The obtained Si/C composite electrode material shows improved rate capability and cycle stability. This synthesis technique can also be used as a general method in preparing other kinds of carbon-coated composites.

Experimental

All chemicals were of analytical grade and purchased from Sinopharm Chemical Reagent Co., Ltd., China.

The graphite (natural graphite, 0.3 g, 1–2 μm) and commercial silicon (0.7 g, 200 mesh) were firstly mixed with polyethylene glycol (10 g, with a molecular weight of 10,000) solution, and then sealed in an 80-mL stainless-steel container filled with argon gas. The above mixture was ball-milled in a high-energy shaker mill (Qinhuangdao Taiji Ring Nano-Products Co., Ltd) at 500 rpm for 10 h using zirconia balls (Ø6 mm in diameter) with the ball to powder weight ratio of 15:1. Afterwards, the as-prepared colloids were quickly frozen by liquid nitrogen and dried in a vacuum condition (10–30 mbars) at −60 °C for about 20 h. Finally, the precursor was heat-treated at 700 °C for 4 h under argon atmosphere at a heating rate of 5 °C min^{-1} followed by natural cooling down. The as-obtained carbon-coated silicon/graphite composite was denoted as nano-Si/C, while the sample prepared under the same conditions and directly dried in the oven at 80 °C was referred as Si/C. In addition, the pure Si with a similar particle size (30–50 nm) was referred as Bare-Si.

X-ray power diffraction (XRD) measurements were performed using an AXS D8 Advance diffractometer (reflection θ-θ geometry, Cu Kα radiation, receiving slit 0.2 mm, scintillation counter, 40 mA, 40 kV) from Bruker, Inc. (Germany). The morphology and structure of the Si/C composite were analyzed by a Hitachi S-4800 field emission scanning electron microscope (FESEM) and an FEI Tecnai G^2 F20 transmission electron microscopy (TEM). The content of carbon in Si–C composites was determined by a Pyris Diamond TG/DTA instrument.

Electrochemical performances were evaluated with a CR2032-type coin cells using lithium metal as counter and reference electrodes, Celgard 2600 as the separator, and 1 M $LiPF_6$ (dissolved in ethylene carbonate and dimethyl carbonate with a 1:1 volume ratio) as the electrolyte. The working electrode was composed of 80 wt.% active materials, 10 wt.% Super P, and 10 wt.% polyvinylidene fluoride. All the cells were activated at a current density of 100 mA g^{-1} for the first cycle and then cycled under different current densities within the voltage range of 0.02–1.2 V using a LAND-CT2001A battery test system (Jinnuo Wuhan Corp., China). Electrochemical impedance spectroscopy analysis was performed using an Autolab PGSTAT302N electrochemical workstation within the frequency range of 0.01 to 100 kHz.

Results and discussion

The nano-Si/C and Si/C composite after carbonization were examined by XRD patterns. The crystal form of silicon and graphite did not change after milling for 10 h and heat-treatment, and any other phases such as silicon carbide did not formed as well. However, a small peak of zirconium dioxide (ZrO_2) arising as a contaminant is found, which is difficult to avoid during high-energy shaker milling. There are a few reports on coating ZrO_2 thin film on the surface of the electrodes to improve their electrochemical performances [25–27]. Herein, whether the small amount of zirconium dioxide will influence the rate performance and cycling

stability of the Si-based composite anode is still up in the air and further studies are desirable.

The morphology and microstructure of as-prepared samples were observed by SEM and TEM analyses. Figure 1a and b present the morphology of nano-Si/C and Si/C composites before the carbonization of PEG. It can be seen that the Si/C composite exhibited a plate-like morphology while the nano-Si/C composite displayed a smaller particle size with nonuniform shapes. After the PEG was pyrolyzed, the nano-Si/C composite showed the smaller particle distribution and more homogeneous carbon-coated layer (Fig. 1c and d). The TEM images investigated that the nano-Si/C composite showed a carbon thin film on its surface with a uniform thickness of about 5 nm, as indicate in Fig. 1e and f, which enabled the sample to form a core-shell structure with primary particles in the range of nano-size (~20 nm). However, the Si/C without freeze-drying exhibited aggregated particles with the primary size of about 300 nm (Fig. 1g). Based on the TG analysis, the as-milled samples were chosen to be heat-treated at 700 °C for 4 h in Ar to decompose the PEG completely, resulting in a yield of carbon residue of 1.8 wt.%. And the residual carbon was coated on surface of the nano-Si/C composite after pyrolysis. This low-carbon residue was reported to be beneficial to improving electrode performance, which contributed to reduce the first irreversible capacity loss due to the formation of a very thin solid electrolyte interphase (SEI) layer on the surface of nano-Si/C composite [28].

The Brunauer–Emmett–Teller test showed that the nano-Si/C sample had a specific surface area of 47.3 $m^2\ g^{-1}$, which was more than five times than that of the Si/C (8.9 $m^2\ g^{-1}$). It is clear that the significant increase in the surface area would be helpful for the liquid electrolyte to penetrate into the particle interspaces, resulting in a high accessibility between of the active material and electrolyte. In addition, the very small grain sizes of the nano-Si/C primary particles could supply faster Li^+-ion diffusion rate because of the shorter charge transfer pathway [29]. Moreover, fluffy structure of the nano-Si/C sample possessed more free space to buffer the volume changes of Li_xSi during discharge and charge.

Figure 2a presents the first discharge–charge profile of the nano-Si/C, Si/C, and Bare-Si electrodes at the current density of 100 mA g^{-1}, respectively. It can be seen that the nano-Si/C

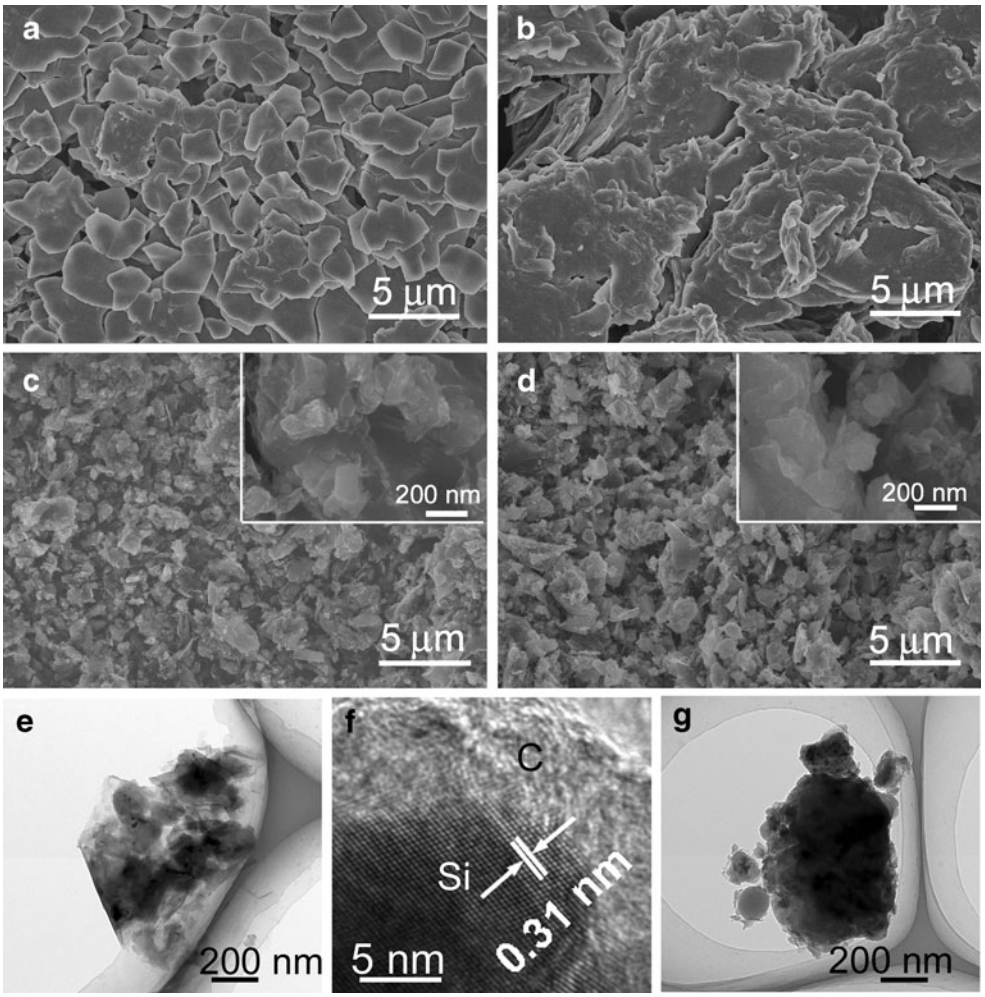

Fig. 1 **a**, **b** FESEM images of nano-Si/C and Si/C samples before pyrolyzing, respectively. **c**, **d** FESEM images of nano-Si/C and Si/C samples after pyrolyzing, respectively. **e**, **f** TEM and high-resolution TEM images of the nano-Si/C composite after pyrolyzed. **g** A TEM image of the Si/C sample after pyrolyzed

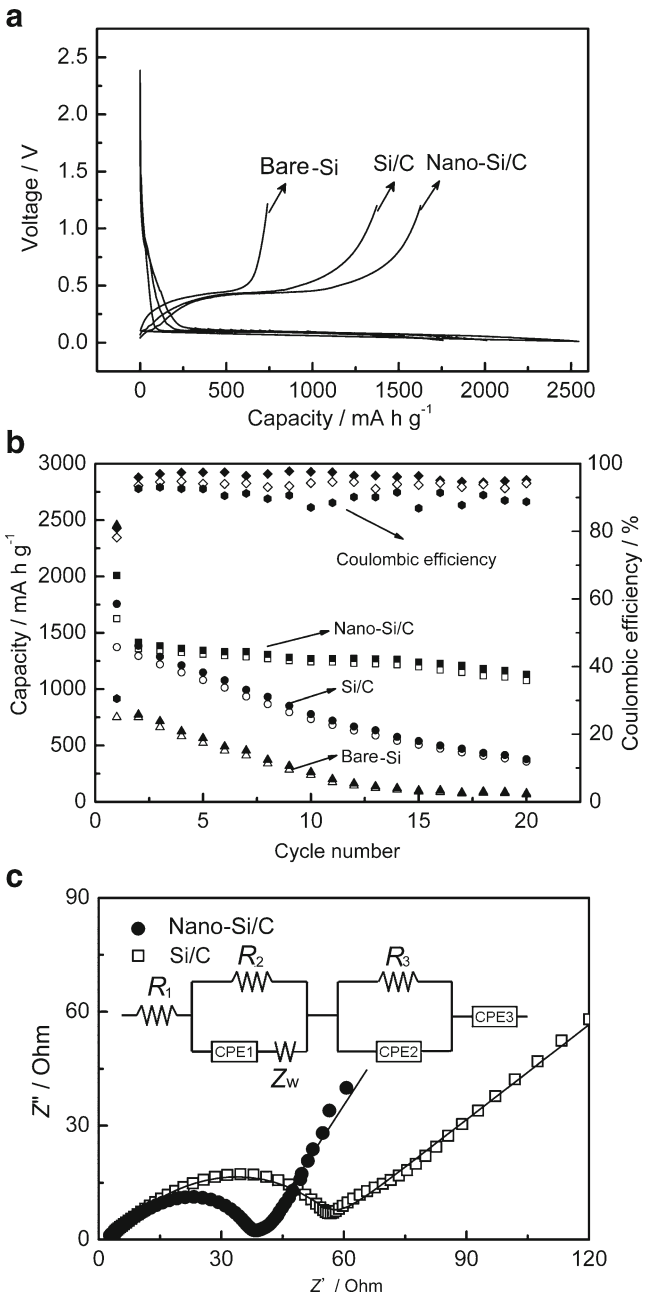

Fig. 2 **a** The first charge and discharge curves of the nano-Si/C, Si/C and bare-Si. **b** Capacity vs. cycle number of nano-Si/C, Si/C, and bare-Si cycled at 100 mA g^{-1}. **c** Nyquist plots of nano-Si/C and Si/C electrodes discharged to 0.09 V (vs. Li/Li^+) at room temperature. Equivalent circuit model of the Si-based anode/Li cell is *inset*

delivered an initial discharge capacity of 2,009 mA h g^{-1} and charge capacity of 1,627 mA h g^{-1}, with a first coulombic efficiency of about 82%. While the Si/C showed a lower first discharge and charge capacity of 1,757 mA h g^{-1} and 1,371 mA h g^{-1}, respectively. In contrast, the Bare-Si exhibited the highest first discharge capacity of 2,540 mA h g^{-1} and the lowest first coulombic efficiency of about 30%. The larger irreversible capacity of Bare-Si should originate from the poor electronic contact between Si particles [7]. After 20 cycles, the nano-Si/C electrode could retain the charge capacity of 1,076 mA h g^{-1}, which is much higher than that of Si/C electrode cycled under the same conditions, as shown in Fig. 2b. While the capacity of Bare-Si electrode degraded so fast that the capacity of only 73 mA h g^{-1} was obtained after 20 cycles. The poor capacity retention might result from the large volume expansion in Si during Li insertion [7]. The coulombic efficiency of nano-Si/C after the first cycle is maintained at about 98% which is much higher than that of the Si/C. The better capacity retention was obtained for the nano-Si/C composite material because of two favorable factors. On the one hand, the graphite in the nano-Si/C material and the fluffy structure introduced by freeze-drying acted as a framework to stabilize the electrode structure during lithiation and delithiation. On the other hand, the coated carbon with uniform distribution could prevent forming nonuniform SEI layer at the beginning of insertion of Li^+ on the surface of Si particles [17–19].

Figure 2c shows the Nyquist plots of the nano-Si/C and Si/C samples discharged to 0.09 V vs. Li/Li^+ after the first cycle. Both of Nyquist plots consist of one depressed semicircle in the medium-frequency region with a straight line in the low-frequency region. The plots can be satisfactorily simulated by an equivalent circuit consisting of an electrolyte resistance in series with a Randles-type impedance element and a blocking CPE as shown in the inset of Fig. 2c [30, 31]. In the equivalent circuit, CPE1 is the constant phase element for the Si–C/electrolyte interface, R_1 is the charge transfer resistance at the Si–C/electrolyte interface, Z_w is the generalized Warburg impedance, CPE2 is the constant phase element for the Si/C interface, R_2 is the electrolyte resistance at the Si/C interface, CPE3 is the constant phase element for the grain-boundary of Si powders, R_3 is the charge transfer resistance between Si grains. The major part of the semicircle usually corresponds to the charge transfer resistance (R_{ct}) at active material/electrolyte interface. The calculated values of R_{ct} were 39 Ω and 61 Ω for the nano-Si/C and Si/C composite electrode, respectively, demonstrating an obviously enhanced charge transfer capability for the nano-Si/C composite in the current half battery.

Cyclic voltammetry (CV) was carried out to identify the characteristics of the redox reactions during charge/discharge cycles. As can be seen in Fig. 3, the first cycle differ from those followed. It is proposed that the reduction peak at around 0.4–0.6 V may be ascribe to the formation of solid electrolyte interface layers on the surface of active materials [32]. This peak disappear after first cycle, indicating that silicon as the anode material in lithium-ion battery has the similar reactive process during the first intercalation of Li^+ into the host material as that for the typical graphite [22]. After the first cycle, the scans displayed a repeatable shape.

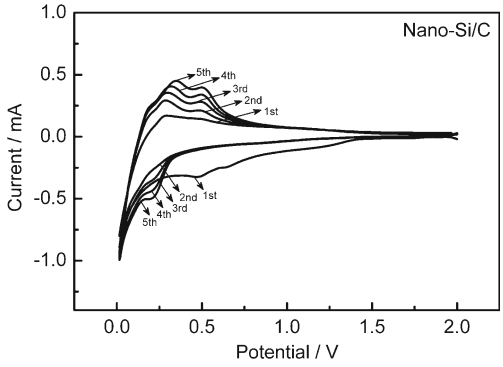

Fig. 3 Cyclic voltammogram curves of nano-Si/C electrode from the first cycle to the fifth cycle at a scan rate of 0.1 mV/s in the voltage range of 0.0 to 2.0 V

And the reduction peak at around 0.0–0.2 V corresponds to the insertion of lithium ions into the host structure of the silicon and graphite materials. In the subsequent cycles, two anodic peaks, located at 0.3 and 0.5 V, respectively, became gradually clear in the anode branches of CV curves, which were attributed to the de-alloying process of Li_xSi alloys.

The statements above give us convincing evidence that the nano-Si/C could provide good charge transport capability and possibly charming surface activities, which would no doubt improve the rate performance of electrode materials. As shown in Fig. 4, the charge capacities of the nano-Si/C are 1,358, 1,136, 1,043, 730, and 472 mA h g^{-1} under various current densities ranging from 100 to 1,000 mA g^{-1}, respectively. It is definite that the unique feature of Si-based electrodes is the voltage plateau between 0.3 and 0.5 V. For the nano-Si/C anode, the charge plateau also was observed even at a high charge current density as high as 1,000 mA g^{-1}. At the same time, when the current increase to 1,000 mA g^{-1}, the nano-Si/C still showed a capacity much higher than that of the commercial graphite anode. Figure 5a shows the first charge capacity of 731.7 and 478 mA h g^{-1} for the nano-Si/C

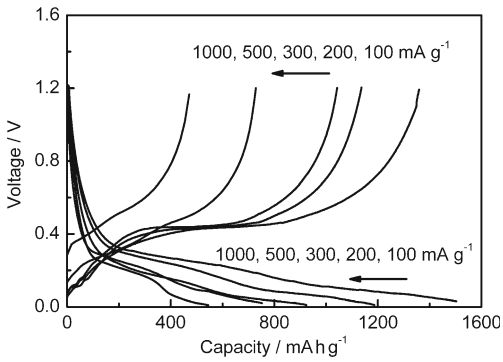

Fig. 4 Galvanostatic discharge/charge curves (Li insertion, voltage decrease; Li extraction, voltage increase, respectively) of nano-Si/C composite at different current densities

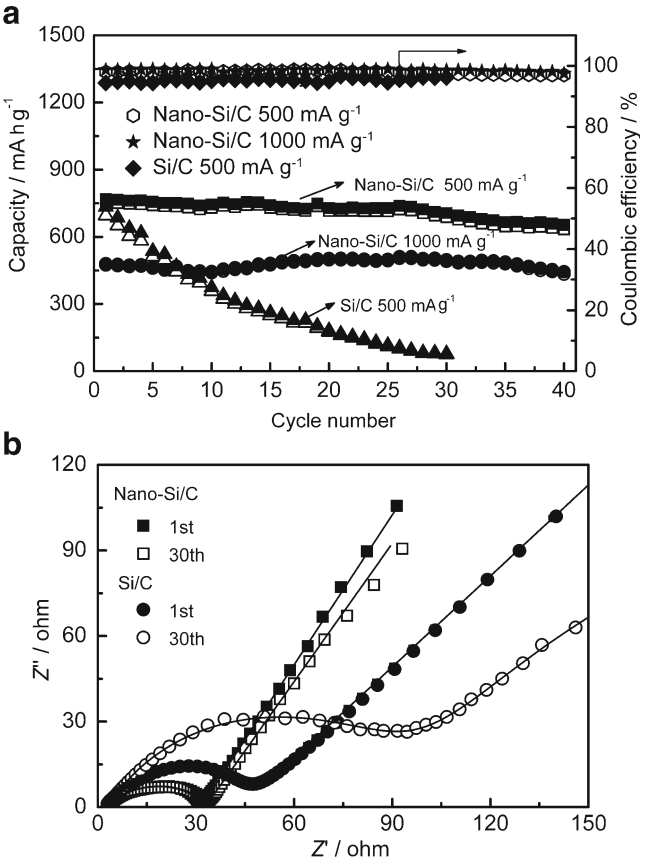

Fig. 5 **a** Capacity vs. cycle number of nano-Si/C and Si/C composites cycled at high current densities. **b** Nyquist plots of nano-Si/C and Si/C electrodes at room temperature

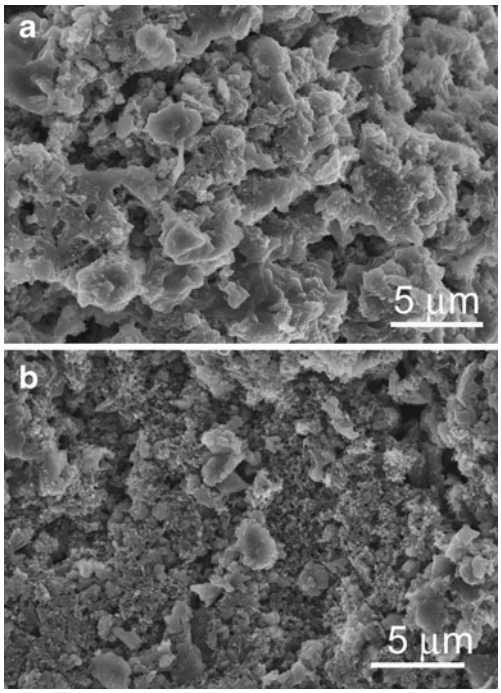

Fig. 6 SEM images of nano-Si/C (**a**) and Si/C (**b**) electrodes after the 30th cycle at 500 mA g^{-1}

composite at 500 and 1,000 mA g^{-1} after activation, respectively. After 40 cycles, the discharge/charge capacity showed little life fading under different current densities. However, the capacity of Si/C composite quickly decreases from 696 to 76 mA h g^{-1} after 30 cycles at 500 mA g^{-1}. These have been well validated by the Nyquist plots of the two different samples in Fig. 5b. It can be clearly found that the calculated R_{ct} only increased from 29 to 31 Ω for the nano-Si/C electrode cycled at 500 mA g^{-1}. This small change in R_{ct} might be due to the better structure stability to release volume change during charge–discharge for the nano-Si/C [33]. In the case of the Si/C material, the R_{ct} increased from 42 to 230 Ω after 30 cycles at 500 mA g^{-1}, which was responsible for the apparent capacity degradation with cycling. These results provide important insight in how to use nano-Si/C material as a high power density anode in LIBs for electrical vehicle and other electronic power source applications.

In order to explain the effect of the freeze-drying on the Si/C composites, it is important to compare the microstructural changes after the cycling tests. The SEM images of nano-Si/C and Si/C composites after the cycling measurement are presented on Fig. 6. The structural difference between the two electrodes can be clearly distinguished. The nano-Si/C electrode maintained the carbon-coated structured and no break of the electrode is observed. However, the pulverization of the Si/C electrode materials was obvious, which lead to poor cycling performance.

Conclusions

In summary, a nanostructured Si/C composite electrode, using as a high capacity anode with good high-rate capability and capacity retention, was obtained by a facile milling and freeze-drying process. The nano-Si/C composite showed higher reversible capacity, better cycling stability, and lower initial irreversible capacity than those of the corresponding sample (Si/C composite) prepared from the normal drying. And the rate performance of nano-Si/C composite was much higher than that of the carbon-based counterparts. The good electrochemical properties should be attributed to the formation of especially fluffy carbon-coated core-shell structure in the course of freeze-drying, which made it attractive to act as a high-performance anode material in the next generation LIBs.

Acknowledgments We are grateful for financial support from the National Natural Science Foundation of China (grant no. 51172250) and the Zhejiang Provincial Natural Science Foundation of China (grant no. R4100194 and Y4100499).

References

1. Armand M, Tarascon JM (2008) Nature 451:652–657
2. Liu HK, Guo ZP, Wang JZ, Konstantinov K (2010) J Mater Chem 20:10055–10057
3. Xiao J, Xu W, Wang DY, Choi DW, Wang W, Li XL, Graff GL, Liu J, Zhang JG (2010) J Electrochem Soc 157:A1047–A1051
4. Yoshio M, Tsumura T, Dimov N (2005) J Power Sources 146:10–14
5. Kim H, Seo M, Park MH, Cho J (2010) Angew Chem Int Ed 49:2146–2149
6. Magasinski A, Dixon P, Hertzberg B, Kvit A, Ayala J, Yushin G (2010) Nat Mater 9:461–461
7. Kasavajjula U, Wang CS, Appleby AJ (2007) J Power Sources 163:1003–1039
8. Larcher D, Beattie S, Morcrette M, Edstroem K, Jumas JC, Tarascon JM (2007) J Mater Chem 17:3759–3772
9. Beattie SD, Larcher D, Morcrette M, Simon B, Tarascon JM (2008) J Electrochem Soc 17:A158–A163
10. Chan CK, Peng H, Liu G, McIlwrath K, Zhang XF, Huggins RA, Cui Y (2008) Nat Nanotechnol 3:31–35
11. Holzapfel M, Buqa H, Hardwick LJ, Hahn M, Wursig A, Scheifele W, Novak P, Kotz R, Veit C, Petrat FM (2006) Electrochem Acta 52:973–978
12. Arie AA, Chang W, Lee JK (2010) J Solid State Electrochem 14:51–56
13. Chen H, Dong Z, Fu Y, Yang Y (2010) J Solid State Electrochem 14:1829–1834
14. Si Q, Hanai K, Imanishi N, Kubo M, Hirano A, Takeda Y, Yamamoto O (2009) J Power Sources 189:761–765
15. Lee JH, Kim WJ, Kim JY, Lim SH, Lee SM (2008) J Power Sources 176:353–358
16. Wang W, Datta MK, Kumta PN (2007) J Mater Chem 17:3229–3237
17. Yang J, Wang BF, Wang K, Liu Y, Xie JY, Wen ZS (2003) Electrochem Solid-State Lett 6:A154–A156
18. Yen YC, Chao SC, Wu HC, Wu NL (2009) J Electrochem Soc 156: A95–A102
19. Fan X, Zou L, Zheng YP, Kang FY, Shen WC (2009) Electrochem Solid-State Lett 12:A199–A201
20. Hasegawa T, Mukai SR, Shirato Y, Tamon H (2004) Carbon 42:2573–2579
21. Yoshio M, Wang HY, Fukuda K (2003) Angew Chem Int Ed 42:4203–4206
22. Wang GX, Ahn JH, Yao J, Bewlay S, Liu HK (2004) Electrochem Commmun 6:689–692
23. Dimov N, Kugino S, Yoshio M (2003) Electrochim Acta 48:1579–1587
24. Deng ZY, Fernandes HR, Ventura JM, Kannan S, Ferreira JMF (2007) J Am Ceram Soc 90:1265–1268
25. Thackeray MM, Johnson CS, Kim JS, Lauzze KC, Vaughey JT, Dietz N, Abraham D, Hackney SA, Zeltner W, Anderson MA (2003) Electrochem Commun 5:752–758
26. Shi DQ, Tu JP, Yuan YF, Wu HM, Li Y, Zhao XB (2006) Electrochem Commun 8:1610–1614
27. Hu SK, Cheng GH, Cheng MY, Hwang BJ, Santhanam R (2009) J Power Sources 188:564–569
28. Wang W, Kumta PN (2007) J Power Sources 172:650–658
29. Oumellal Y, Delpuech N, Mazouzi D, Dupre N, Gaubicher J, Moreau P, Soudan P, Lestriez B, Guyomard D (2011) J Mater Chem 21:6201–6208
30. Liu WR, Wang JH, Wu HC, Shieh DT, Yang MH, Wu NL (2005) J Electrochem Soc 152:A1719–A1725
31. Chou SL, Wang JZ, Choucair M, Liu HK, Stride JA, Dou SX (2010) Electrochem Commmun 12:303–306
32. Khomenko VG, Barsukov VZ (2007) Electrochem Acta 52:2829–2840
33. Guo JC, Chen XL, Wang CS (2010) J Mater Chem 20:5035–5040